JACS
JOURNAL OF THE AMERICAN CHEMICAL SOCIETY

Subscriber access provided by ISTANBUL TEKNIK UNIV

Article

Onset of 3-Helical Secondary Structure in Aib Oligopeptides Probed by Coherent 2D IR Spectroscopy

Hiroaki Maekawa, Fernando Formaggio, Claudio Toniolo, and Nien-Hui Ge

J. Am. Chem. Soc., **2008**, 130 (20), 6556-6566 • DOI: 10.1021/ja8007165 • Publication Date (Web): 29 April 2008

Downloaded from http://pubs.acs.org on February 8, 2009

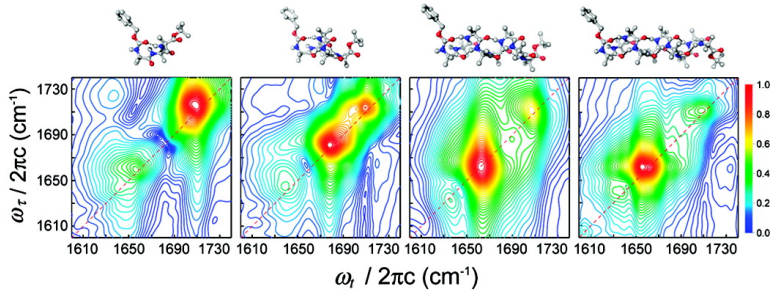

More About This Article

Additional resources and features associated with this article are available within the HTML version:

- Supporting Information
- Links to the 1 articles that cite this article, as of the time of this article download
- Access to high resolution figures
- Links to articles and content related to this article
- Copyright permission to reproduce figures and/or text from this article

View the Full Text HTML

ACS Publications
High quality. High impact.

Journal of the American Chemical Society is published by the American Chemical Society. 1155 Sixteenth Street N.W., Washington, DC 20036

J|A|C|S
ARTICLES

Published on Web 04/29/2008

Onset of 3_{10}-Helical Secondary Structure in Aib Oligopeptides Probed by Coherent 2D IR Spectroscopy

Hiroaki Maekawa,[†] Fernando Formaggio,[‡] Claudio Toniolo,[‡] and Nien-Hui Ge*,[†]

Department of Chemistry, University of California at Irvine, Irvine, California 92697-2025 and Institute of Biomolecular Chemistry, CNR, Padova Unit, Department of Chemistry, University of Padova, 35131 Padova, Italy

Received January 29, 2008; E-mail: nhge@uci.edu

Abstract: We have investigated the onset of the secondary structure and the evolution of two-dimensional infrared (2D IR) spectral patterns as a function of chain length with a study of 3_{10}-helical peptides. The results show that 2D IR is highly sensitive to peptide conformation, disorder, and size. An extensive set of 2D IR spectra of C^{α}-methylated homopeptides, Z-(Aib)$_n$-O*t*Bu ($n = 3$, 5, 8, and 10), in $CDCl_3$ was measured in the amide-I region. The 2D spectral patterns of the tripeptide are quite different from those of the longer peptides. The spectral signatures begin to converge at the pentapeptide and become almost the same for the octa- and decapeptide. Simulations employing a vibrational exciton model were performed, with the local mode frequency shifts estimated from the intramolecular hydrogen bond electrostatic energies. The 2D spectra are well simulated using dihedral angle distributions around the average values $(\phi, \psi) \approx (-57°, -31°)$ with a width of $\sim 21°$. The simulated site-dependent amide-I local mode frequencies are in agreement with those from scaled semiempirical AM1 calculations. The tripeptide exhibits a more noticeable discrepancy between the experimental and simulated cross-peak patterns. This behavior suggests the presence of a peptide population outside the single β-turn conformation. The onset of the 3_{10}-helical secondary structure appears to already occur at the pentapeptide level.

Introduction

The 3_{10}-helix is the third principal secondary structural element that occurs in globular proteins, beside the α-helix and β-sheet.[1,2] The intramolecular C═O···H—N bonding pattern is of the $i \leftarrow (i + 3)$ type in the 3_{10}-helix, whereas it is $i \leftarrow (i + 4)$ in the α-helix. The 3_{10}-helices commonly observed in proteins are rather short, 3.3 residues on average.[3] A more recent survey revealed novel protein structural motifs containing two- to three-turn 3_{10}-helices.[4] The 3_{10}-helix has been shown to play an important biochemical role.[5–7] A considerable amount of evidence indicates that the 3_{10}-helix is a thermodynamic intermediate in α-helix folding.[8,9] Simulations indicate that the conformational transitions between 3_{10}- and α-helices occur on picosecond timescales.[10–12] Due to the importance of the 3_{10}-helix, there has been a great deal of interest in trying to detect the onset of the 3_{10}-helical structure and to understand how chain length, amino acid composition, and exact sequence affect the preferences for 3_{10}-helix formation.[13–21]

Many of these studies investigated the Aib (α-aminoisobutyric acid or $C^{\alpha,\alpha}$-dimethylglycine) containing peptides.[13–18] Aib occurs extensively in membrane-active peptaibol antibiotics, such as alamethicin.[22,23] Because of the steric interactions of the *gem*-methyl groups attached to the α-carbon, Aib residues

[†] University of California at Irvine.
[‡] University of Padova.

(1) Toniolo, C.; Benedetti, E. *Trends Biochem. Sci.* **1991**, *16*, 350.
(2) Bolin, K. A.; Millhauser, G. L. *Acc. Chem. Res.* **1999**, *32*, 1027.
(3) Barlow, D. J.; Thornton, J. M. *J. Mol. Biol.* **1988**, *201*, 601.
(4) Pal, L.; Basu, G. *Protein Eng.* **1999**, *12*, 811.
(5) De Guzman, R. N.; Wu, Z. R.; Stalling, C. C.; Pappalardo, L.; Borer, P. N.; Summers, M. F. *Science* **1998**, *279*, 384.
(6) Hashimoto, Y.; Kohri, K.; Kaneko, Y.; Morisaki, H.; Kato, T.; Ikeda, K.; Nakanishi, M. *J. Biol. Chem.* **1998**, *273*, 16544.
(7) Matsushima, N.; Enkhbayar, P.; Kamiya, M.; Osaki, M.; Kretsinger, R. H. *Drug Des. Rev.—Online* **2005**, *2*, 305.
(8) Millhauser, G. L. *Biochemistry* **1995**, *34*, 3873.
(9) Shea, J. E.; Brooks, C. L. *Annu. Rev. Phys. Chem.* **2001**, *52*, 499.
(10) Tirado-Rives, J.; Jorgensen, W. L. *Biochemistry* **1991**, *30*, 3864.
(11) Soman, K. V.; Karimi, A.; Case, D. A. *Biopolymers* **1991**, *31*, 1351.
(12) Pengo, P.; Pasquato, L.; Moro, S.; Brigo, A.; Fogolari, F.; Broxterman, Q. B.; Kaptein, B.; Scrimin, P. *Angew. Chem., Int. Ed.* **2003**, *42*, 3388.
(13) Karle, I. L.; Balaram, P. *Biochemistry* **1990**, *29*, 6747.
(14) Toniolo, C.; Crisma, M.; Formaggio, F.; Peggion, C. *Biopolymers* **2001**, *60*, 396.
(15) Toniolo, C.; Bonora, G. M.; Barone, V.; Bavoso, A.; Benedetti, E.; Di Blasio, B.; Grimaldi, P.; Lelj, F.; Pavone, V.; Pedone, C. *Macromolecules* **1985**, *18*, 895.
(16) Kennedy, D. F.; Crisma, M.; Toniolo, C.; Chapman, D. *Biochemistry* **1991**, *30*, 6541.
(17) Silva, R. A. G. D.; Yasui, S. C.; Kubelka, J.; Formaggio, F.; Crisma, M.; Toniolo, C.; Keiderling, T. A. *Biopolymers* **2002**, *65*, 229.
(18) Marshall, G. R.; Hodgkin, E. E.; Langs, D. A.; Smith, G. D.; Zabrocki, J.; Leplawy, M. T. *Proc. Natl. Acad. Sci. U.S.A.* **1990**, *87*, 487.
(19) Crisma, M.; Bisson, W.; Formaggio, F.; Broxterman, Q. B.; Toniolo, C. *Biopolymers* **2002**, *64*, 236.
(20) Yoder, G.; Polese, A.; Silva, R. A. G. D.; Formaggio, F.; Crisma, M.; Broxterman, Q. B.; Kamphuis, J.; Toniolo, C.; Keiderling, T. A. *J. Am. Chem. Soc.* **1997**, *119*, 10278.
(21) Tanaka, M. *Chem. Pharm. Bull.* **2007**, *55*, 349.
(22) Nagaraj, R.; Balaram, P. *Acc. Chem. Res.* **1981**, *14*, 356.
(23) Degenkolb, T.; Kirschbaum, J.; Brueckner, H. *Chem. Biodiversity* **2007**, *4*, 1052.
(24) Paterson, Y.; Rumsey, S. M.; Benedetti, E.; Némethy, G.; Scheraga, H. A. *J. Am. Chem. Soc.* **1981**, *103*, 2947.
(25) Improta, R.; Barone, V.; Kudin, K. N.; Scuseria, G. E. *J. Am. Chem. Soc.* **2001**, *123*, 3311.
(26) Marshall, G. R. *In Intra-Science Chemistry Reports*; Kharasch, N., Ed.; Gordon & Breach: New York, 1971; pp 305–316.

 10.1021/ja8007165 CCC: $40.75 © **2008 American Chemical Society**

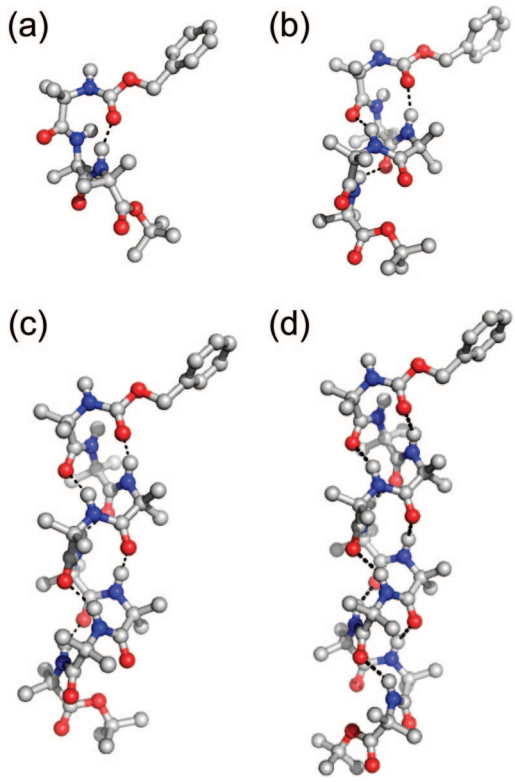

Figure 1. Computer-drawn molecular structures of Z-$(Aib)_n$-O*t*Bu forming an ideal 3_{10}-helix [$(\varphi, \psi) = (-57°, -30°)$]:[1] $n = 3$ (a); 5 (b); 8 (c); and 10 (d). Hydrogen atoms of the capping groups and the methyl groups on the C^{α}-carbon atoms are omitted. The intramolecular C═O···H—N hydrogen bonds between the i and $(i + 3)$ residues are indicated by the dashed lines. The structure of $n = 3$ corresponds to a single type-III β-turn forming a 10-membered ring.

are energetically limited to a narrow region of conformational space.[24–26] The structural rigidity of Aib and its high helical propensity make Aib-containing oligopeptides attractive models for developing and refining experimental and theoretical approaches to peptide conformational analysis. Several Aib-rich oligopeptide systems have been reported to serve as a good model for the 3_{10}-helix, and their chain length dependent FT IR, ^{1}H NMR, electronic and vibrational circular dichroism (ECD and VCD) spectra have been measured.[15–17] Aib homopeptides of various lengths were shown to form the 3_{10}-helix in weakly polar solvents such as $CDCl_3$, as well as in the crystal state.[15,16,27–31] The propensity of Aib residues to initiate type-III (III′) β-turns[32] was demonstrated in small end-capped Aib peptides even with as few as three residues[28,33] (Figure 1a).

A great deal of insight has been obtained from these conventional techniques. However, NMR, ECD, and VCD do not have sufficient time resolutions to study the role of the 3_{10}-helix during the earliest steps of the helix formation processes. Although time-resolved linear IR spectroscopy can be performed on femtosecond and picosecond time scales, the correlation between linear IR spectra and peptide structures remains largely qualitative. For example, the amide-I mode, involving primarily the C═O stretching of the peptide unit, has been extensively used to identify secondary structure motifs.[34] However, the amide-I peak maximum cannot be used to discriminate between 3_{10}- and α-helices.[17,35] Moreover, we believe that some unresolved issues exist in the practice of using the chain length dependence of the ratio of the integrated linear IR absorbances of hydrogen-bonded N—H groups (A_b) to the free N—H group (A_f) to elucidate the solution conformation of 3_{10}-helical peptides.[15,28,29,36] For a short peptide, the ratio of $(A_b/A_f)/(n-2)$ as a function of the chain length (n) may not follow a simple constant relation as expected for a complete 3_{10}-helix. This deviation has been attributed to the lower percent population of the 3_{10}-helical conformation for a shorter chain length.[15] It is also possible that the deviation is because the short peptide populates an intramolecularly hydrogen-bonded 3_{10}-helical conformation with a chain length dependent distortion that results in variations in molar extinction coefficients of the hydrogen-bonded N—H groups.[36] This ambiguity illustrates yet another difficulty in extracting structural information from linear IR spectra.

Femtosecond two-dimensional infrared (2D IR) spectroscopy of the amide-I mode[37–58] can overcome a number of these difficulties in studying peptides with linear IR spectroscopy. Going beyond one dimension in a manner similar to that for

(27) Gessmann, R.; Brueckner, H.; Petratos, K. *J. Peptide Sci.* **2003**, *9*, 753.
(28) Benedetti, E.; Bavoso, A.; Di Blasio, B.; Pavone, V.; Pedone, C.; Crisma, M.; Bonora, G. M.; Toniolo, C. *J. Am. Chem. Soc.* **1982**, *104*, 2437.
(29) Bonora, G. M.; Mapelli, C.; Toniolo, C.; Wilkening, R. R.; Stevens, E. S. *Int. J. Biol. Macromol.* **1984**, *6*, 179.
(30) Toniolo, C.; Bonora, G. M.; Bavoso, A.; Benedetti, E.; Di Blasio, B.; Pavone, V.; Pedone, C. *Macromolecules* **1986**, *19*, 472.
(31) Toniolo, C.; Crisma, M.; Bonora, G. M.; Benedetti, E.; Di Blasio, B.; Pavone, V.; Pedone, C.; Santini, A. *Biopolymers* **1991**, *31*, 129.
(32) Venkatachalam, C. M. *Biopolymers* **1968**, *6*, 1425.
(33) Rao, C. P.; Nagaraj, R.; Rao, C. N. R.; Balaram, P. *Biochemistry* **1980**, *19*, 425.
(34) Krimm, S.; Bandekar, J. *Adv. Protein Chem.* **1986**, *38*, 181.
(35) Martinez, G.; Millhauser, G. *J. Struct. Biol.* **1995**, *114*, 23.
(36) Pispisa, B.; Palleschi, A.; Stella, L.; Venanzi, M.; Mazzuca, C.; Formaggio, F.; Toniolo, C.; Broxterman, Q. B. *J. Phys. Chem. B* **2002**, *106*, 5733.
(37) Hamm, P.; Lim, M.; Hochstrasser, R. M. *J. Phys. Chem. B* **1998**, *102*, 6123.
(38) Asplund, M. C.; Zanni, M. T.; Hochstrasser, R. M. *Proc. Natl. Acad. Sci. U.S.A.* **2000**, *97*, 8219.
(39) Woutersen, S.; Hamm, P. *J. Chem. Phys.* **2001**, *115*, 7737.
(40) Woutersen, S.; Hamm, P. *J. Phys.: Condens. Matter* **2002**, *14*, R1035.
(41) Sul, S.; Karaiskaj, D.; Jiang, Y.; Ge, N.-H. *J. Phys. Chem. B* **2006**, *110*, 19891.
(42) Demirdöven, N.; Cheatum, C. M.; Chung, H. S.; Khalil, M.; Knoester, J.; Tokmakoff, A. *J. Am. Chem. Soc.* **2004**, *126*, 7981.
(43) Wang, J.; Chen, J.; Hochstrasser, R. M. *J. Phys. Chem. B* **2006**, *110*, 7545.
(44) Smith, W. S.; Tokmakoff, A. *J. Chem. Phys.* **2007**, *126*, 045109.
(45) Maekawa, H.; Toniolo, C.; Moretto, A.; Broxterman, Q. B.; Ge, N.-H. *J. Phys. Chem. B* **2006**, *110*, 5834.
(46) Maekawa, H.; Toniolo, C.; Broxterman, Q. B.; Ge, N.-H. *J. Phys. Chem. B* **2007**, *111*, 3222.
(47) Fang, C.; Senes, A.; Cristian, L.; DeGrado, W. F.; Hochstrasser, R. M. *Proc. Natl. Acad. Sci. U.S.A.* **2006**, *103*, 16740.
(48) Rubtsov, I. V.; Wang, J.; Hochstrasser, R. M. *Proc. Natl. Acad. Sci. U.S.A.* **2003**, *100*, 5601.
(49) Rubtsov, I. V.; Wang, J.; Hochstrasser, R. M. *J. Phys. Chem. A* **2003**, *107*, 3384.
(50) Bredenbeck, J.; Helbing, J.; Kumita, J. R.; Woolley, G. A.; Hamm, P. *Proc. Natl. Acad. Sci. U.S.A.* **2005**, *102*, 2379.
(51) Kolano, C.; Helbing, J.; Kozinski, M.; Sander, W.; Hamm, P. *Nature* **2006**, *444*, 469.
(52) Mukherjee, P.; Kass, I.; Arkin, I. T.; Zanni, M. T. *Proc. Natl. Acad. Sci. U.S.A.* **2006**, *103*, 3528.
(53) Choi, J.-H.; Hahn, S.; Cho, M. *Biopolymers* **2006**, *83*, 519.
(54) Cheatum, C. M.; Tokmakoff, A.; Knoester, J. *J. Chem. Phys.* **2004**, *120*, 8201.
(55) Abramavicius, D.; Zhuang, W.; Mukamel, S. *J. Phys. Chem. B* **2004**, *108*, 18034.
(56) Zhuang, W.; Abramavicius, D.; Mukamel, S. *Proc. Natl. Acad. Sci. U.S.A.* **2005**, *102*, 7443.
(57) Wang, J.; Hochstrasser, R. M. *Chem. Phys.* **2004**, *297*, 195.
(58) Mukamel, S. *Annu. Rev. Phys. Chem.* **2000**, *51*, 691.

2D NMR, 2D IR spectra exhibit cross-peaks that reveal couplings between vibrators. The backbone conformations of small peptides have been determined based on vibrational coupling strengths between the amide-I modes.[37,40,41] Amide-I 2D IR spectra have been shown to be highly structurally sensitive and exhibit spectral patterns that are characteristic of peptide secondary structures.[39,42–46,53–57] A Z-shaped pattern, for example, appears in the 2D absorptive spectra of antiparallel β-sheets and hairpins.[42,44] A clear doublet shows up in the cross-peak pattern of several 3_{10}-helical octapeptides, distinctly different from the multiple peak pattern observed for the mixed $3_{10}/\alpha$-helix.[45,46] The spatial resolution of 2D IR spectroscopy can be enhanced to the residue level by isotope labeling of the peptide carbonyl groups.[43,47] Two-color 2D IR experiments have made it possible to estimate the couplings between the amide-I mode and amide-II/amide-A modes,[48,49] similar in principle to heteronuclear NMR. By taking advantage of the intrinsic picosecond time resolution of 2D IR spectroscopy, transient 2D IR measurements have made important progress in elucidating ultrafast protein folding/unfolding processes.[50,51]

In this work we investigate the onset of the 3_{10}-helical secondary structure and the evolution of 2D IR spectral patterns as a function of chain length with a study of Z-$(Aib)_n$-O*t*Bu (Z, benzyloxycarbonyl; O*t*Bu, *tert*-butoxy, $n = 3$, 5, 8, and 10) in $CDCl_3$. This series of peptides has served as a model system for the study of incipient and fully developed 3_{10}-helices.[15] The number of possible β-turns increases from one ($n = 3$, Figure 1a) to eight ($n = 10$, Figure 1d) over the series. Because a complete turn of the 3_{10}-helix requires three successive $i \leftarrow (i + 3)$ hydrogen bonds, the decapeptide is one hydrogen bond short of forming a three-turn 3_{10}-helix. The aims of our study are two-fold. First, a previous analysis of $(A_b/A_f)/(n-2)$ indicated that a fully developed, stable 3_{10}-helical structure is formed at about the octamer level,[15] whereas earlier studies suggested the tri-, tetra-, and pentapeptides exclusively populate the single, double, and triple β-turn structures.[28,29] A detailed study reconciling these differences is needed. Because we have demonstrated the high sensitivity of 2D IR in distinguishing between 3_{10}- and α-helices,[45,46] a 2D IR study should provide a possible resolution.

Second, in an effort to firmly establish the 2D IR spectrum−structure relationship, one important missing link that still requires systematic experimental investigation is the peptide size dependence of 2D IR spectral patterns. This knowledge is indispensable for studying the secondary structures of short peptides. Moreover, the chain length dependence of 2D spectra at equilibrium provides essential baseline spectral signatures which are needed for proper interpretation of the 2D spectral evolution involved in nonequilibrium protein folding and unfolding processes, as well as the identification of structural intermediates. So far, our understanding of the chain length dependence of 2D IR spectra mainly comes from theoretical studies. Cheatum et al.[54] simulated the 2D absorptive spectra of the β-sheet structure with different sizes based on the vibrational exciton model. We recently simulated the 2D IR cross-peak patterns of ideal 3_{10}-helix peptides with 5, 8, and 11 residues.[46] Clearly, systematic experimental investigations are needed.

Previously, we have reported the 2D IR cross-peak pattern of Z-$(Aib)_8$-O*t*Bu in $CDCl_3$ using the rephasing (R) pulse sequence with the double-crossed polarization configuration.[46] The octapeptide exhibits a doublet cross-peak pattern in the amide-I region, which is assigned as a characteristic of the 3_{10}-helix conformation, as corroborated by our theoretical calculations.[46] Here we present chain length dependent 2D IR spectra of the Aib homopeptides using three different pulse sequences: R, nonrephasing (NR), and reverse photon echo (RPE) sequences under the parallel polarization configuration. Moreover, we measured 2D IR cross-peak patterns using the R sequence with the double-crossed polarization configuration to investigate the size dependence of the doublet pattern. These experiments revealed the evolution of the 2D IR spectral signatures as the chain length progresses.

In the following discussion, we analyze the signatures of the 3_{10}-helix 2D IR spectra in terms of the vibrational couplings and site energies of polypeptides in the helical hydrogen-bonding registry. This discussion is based on comparisons between our experimental results and simulations using a recent model that specifically takes into account the effects of hydrogen bond geometry and origin on the local amide-I frequency.[46] How the extent of vibrational couplings evolves with chain length and its effect on the convergence of 2D spectra are discussed. We compare the site dependency of amide-I local mode frequencies from our simulations with that predicted from AM1 semiempirical calculations and suggest the potential of combining semiempirical calculations and molecular dynamics simulations to effectively simulate 2D spectra. The sensitivity of the simulated parameters to backbone dihedral angles and their variations is explored. The results lead us to conclude that 2D IR spectroscopy can become an important structural probe of protein folding mechanisms, such as in the initial steps of the coil-to-helix transition.

Experimental Procedures

The principles of 2D IR spectroscopy and details of our spectrometer and data processing method have been described previously.[41,45,46] Here we briefly summarize the features relevant to the data discussion below.

In third order 2D IR spectroscopy, three femtosecond IR pulses interact with the sample. The bandwidth of the pulses is sufficient to resonantly excite the fundamental transitions from the ground state to the single-quantum states ($v = 0 \rightarrow 1$) and the anharmonically shifted transitions from the single-quantum to the double-quantum states ($v = 1 \rightarrow 2$). The system freely evolves during the sequential time intervals τ and T between the three pulses, and a generated field emits at time t after the third pulse. For the R and NR sequences, the evolution of 0–1 vibrational coherences is sampled as a function of τ, and that of 0–1 and 1–2 coherences is sampled as a function of t. The 2D Fourier transformed spectra are represented in ω_τ and ω_t, correlating between the single quantum transitions. These two sequences differ in that the coherences evolve with an opposite sign during τ, and hence the 2D R and NR spectra are located in the $-\omega_\tau$ and $+\omega_\tau$ quadrants, respectively. Summing the real parts of R and NR spectra together eliminates the dispersive line shape and gives the 2D absorptive spectrum. For the RPE sequence, two successive excitations create 0–2 coherences that evolve during the T period and the third pulse generates 0–1 and 1–2 coherences for detection during the t period. The RPE spectrum in ω_T and ω_t thus correlates the double quantum transitions with the single quantum transitions.

The experiments were performed by focusing onto the sample three mid-IR pulses (100 fs pulse width, 150 cm^{-1} bandwidth, and 1667 cm^{-1} central frequency) with wavevectors of $\boldsymbol{k}_a$, $\boldsymbol{k}_b$, and $\boldsymbol{k}_c$. The nonlinear signal emitted in the $-\boldsymbol{k}_a + \boldsymbol{k}_b + \boldsymbol{k}_c$ phase-matching direction was heterodyne detected by a local oscillator (LO) pulse. Experimental 2D data were obtained by spectral interferometry utilizing a 64-element mercury−cadmium−telluride array detector attached to a monochromator, with a spectral resolution of ~4 cm^{-1}/pixel. In this detection scheme, the LO pulse was set to

precede the signal field by 800 fs and the monochromator effectively performed a Fourier transform with respect to t. Interferograms were processed following the procedure described by Joffre and co-workers[59] to yield the emitted signal frequency ω_t. For the R (a−b−c) and NR (b−a−c) sequences, τ was scanned from 0 to 2.7 ps and from 0 to 2.25 ps, respectively, with 4.5 fs steps at a fixed $T = 300$ fs. For the RPE (b−c−a) sequence, T was scanned from 0 to 1.8 ps with 4.5 fs steps at a fixed $\tau = 300$ fs. The resulting (τ, ω_t) and (T, ω_t) 2D matrices were Fourier transformed along τ and T to obtain the corresponding 2D spectra in ($\pm\omega_\tau$, ω_t) and (ω_T, ω_t), respectively. The phase of the R and NR spectra was obtained by matching the ω_t-projection of the absorptive spectrum to the dispersed pump–probe spectrum measured at the same delay time as T.[60] The polarization configuration as of the excitation pulses (a, b, c) and the signal (d) is denoted as $\langle a, b, c, d\rangle$.[45,46] For the parallel polarization configuration, $\langle Z, Z, Z, Z\rangle$, we performed experiments using R, NR, and RPE sequences and the nonscanning time delay was set to 300 fs to reduce the nonresonant contributions from the solvent. For the double-crossed polarization configuration, $\langle \pi/4, -\pi/4, Y, Z\rangle$,[41,61] the R sequence was used and T was set to zero.

Linear IR spectra were measured with a purged FT IR spectrometer (Perkin-Elmer, Spectrum 2000). Each spectrum was collected with a 4 cm^{-1} resolution and averaged over 16 scans. Background spectra of the neat solvents were measured under the same conditions and subtracted from the peptide solution spectra.

The Aib homopeptides Z-$(Aib)_n$-OtBu ($n = 3$, 5, 8, and 10) were synthesized and characterized as described previously.[15,62] The peptide concentration in $CDCl_3$ (Cambridge Isotopes Laboratory, 99.96 atom% D) was kept below 10 mM to minimize interpeptide aggregation.[15] The path length of the sample cell was 250 μm, and the optical densities of the amide-I band were 0.15–0.30. All FT IR and 2D IR spectra were measured at ambient temperature (20 °C).

Model Calculations

Linear and 2D IR spectra of the amide-I mode were simulated based on a simple vibrational exciton model that has been widely used to describe the vibrational responses of peptides and proteins.[37,40,43,44,46,52,55] In this model, the vibrational eigenstates were calculated as a set of coupled anharmonic oscillators. The fundamental frequencies of the amide-I local modes ω_p^0 ($p = 1, 2, ..., N$ where N is the number of peptide linkages) were estimated by incorporating several influencing factors into the following equation

$$\omega_p^0 = \omega_0 - \delta\omega_{\text{solvent}} - \delta\omega_{\text{CO}} - \delta\omega_{\text{NH}} = \tilde{\omega}_0 - \delta\omega_{\text{CO}} - \delta\omega_{\text{NH}} \quad (1)$$

Here ω_0 denotes the unperturbed local mode frequency that excludes the effects of intramolecular hydrogen bonding and intermolecular solvation, $\delta\omega_{\text{solvent}}$ describes the frequency shift induced by intermolecular interactions with solvent, and $\delta\omega_{\text{CO(NH)}}$ denotes the frequency shift induced by intramolecular hydrogen bonding at the C═O (N−H) site of the peptide linkage.

Generally speaking, ω_0 is site dependent because each peptide linkage may not have exactly the same local chemical environment due to variations in the surrounding side chains and capping groups. Many previous studies assumed a constant ω_0 over the entire peptide chain for simplicity.[37,42,54,55] However, it is important to take into account the site dependence of ω_0, as implied in several recent studies.[43,44,53] Empirically $\delta\omega_{\text{solvent}}$ is often assumed to be on the order of 10–20 cm^{-1},[44,46,55] and it has a larger value when solvent exposure occurs at the C═O site of a peptide unit as compared to the N−H site. Because there is no simple model to independently estimate ω_0 and $\delta\omega_{\text{solvent}}$ for each site, we lumped them together and defined a single parameter $\tilde{\omega}_0 = \omega_0 - \delta\omega_{\text{solvent}}$. In the simulation, $\tilde{\omega}_0$ was either adjusted or held fixed, depending on the site position and the chain length. To estimate $\delta\omega_{\text{CO(NH)}}$, a new model we developed recently[46] was applied to linearly correlate $\delta\omega_{\text{CO(NH)}}$ to the electrostatic energy (E_{KS}) between the hydrogen-bonded C═O and N−H groups:

$$\delta\omega_{\text{CO}} = 2.4\ \text{cm}^{-1}\ \text{mol/kJ} \times E_{\text{KS}} \quad (2)$$

$$\delta\omega_{\text{NH}} = 1.0\ \text{cm}^{-1}\ \text{mol/kJ} \times E_{\text{KS}} \quad (3)$$

where E_{KS} is the Kabsch−Sander electrostatic energy of hydrogen bond formation.[63]

Two different types of vibrational couplings ($\beta_{p,q}$) between the amide-I oscillators were considered based on whether the local modes were covalently neighbored or not. The nearest neighbor coupling ($\beta_{p,p\pm1}$) was obtained from an *ab initio* map calculated for glycine dipeptide at the RHF/6-311G**(d,p) level by Cho and co-workers.[64] This map was chosen from several available maps for consistency because we obtained the coefficients in eqs 2 and 3 by making a comparison to *ab initio* calculations done at the same level.[65] We tested the performance of this map against another map from Stock and co-workers.[66] The octapeptide 2D spectra calculated based on these two maps exhibit very similar spectral features (data not shown). Couplings between local modes separated by more than one residue were approximated by the transition dipole coupling interactions[34,67] using previous parametrization of the magnitude, position, and orientation of the dipoles.[68] For the two-quantum states, the diagonal anharmonicity of each local mode was set to 16 cm^{-1}, an experimental value measured for N-methyl acetamide (NMA).[37] The couplings between these states were considered to be bilinear under the harmonic approximation.[37]

The one- and two-exciton eigenstates resulting from such a set of coupled oscillators were then used to calculate the transition dipoles and frequencies involved in linear and nonlinear responses. We assumed that the fast fluctuations of the excitonic band frequencies are strictly separated in time scales from the slowly fluctuating inhomogeneities. Although this model is crude, it has been successfully applied to capture the essential amide-I 2D IR spectral features of many systems, including small peptides.[37,40–44,46] The explicit formulas we used for calculating the linear, 2D R and NR spectra have been reported previously.[46] The 2D RPE spectrum $S^{RPE}_{b-c-a}(\omega_T,\omega_t;\tau)$ under the $\langle Z, Z, Z, Z\rangle$ polarization

(59) Dorrer, C.; Belabas, N.; Likforman, J. P.; Joffre, M. *J. Opt. Soc. Am. B* **2000**, *17*, 1795.
(60) Jonas, D. M. *Annu. Rev. Phys. Chem.* **2003**, *54*, 425.
(61) Zanni, M. T.; Ge, N.-H.; Kim, Y. S.; Hochstrasser, R. M. *Proc. Natl. Acad. Sci. U.S.A.* **2001**, *98*, 11265.
(62) Jones, D. S.; Kenner, G. W.; Preston, J.; Sheppard, R. C. *J. Chem. Soc.* **1965**, 6227.
(63) Kabsch, W.; Sander, C. *Biopolymers* **1983**, *22*, 2577.
(64) Ham, S.; Cho, M. *J. Chem. Phys.* **2003**, *118*, 6915.
(65) Kim, J.-H.; Cho, M. *Bull. Korean Chem. Soc.* **2003**, *24*, 1061.
(66) Gorbunov, R. D.; Kosov, D. S.; Stock, G. *J. Chem. Phys.* **2005**, *122*, 224904.
(67) Torii, H.; Tasumi, M. *J. Chem. Phys.* **1992**, *96*, 3379.
(68) Ham, S.; Cha, S.; Choi, J.-H.; Cho, M. *J. Chem. Phys.* **2003**, *119*, 1451.
(69) Oxtoby, D. W. *Annu. Rev. Phys. Chem.* **1981**, *32*, 77.

Table 1. Optimized Parameters for Simulations of 2D IR Spectra of Z-$(Aib)_n$-O*t*Bu in $CDCl_3$ (n = 3, 5, 8, and 10)[a]

		$\bar{\omega}_0$ (σ)/cm^{-1}										
n	(ϕ, ψ) ($\sigma_\phi = \sigma_\psi$)	1	2	3	4	5	6	7	8	9	ω_U (σ_U)/cm^{-1}	ω_E (σ_E)/cm^{-1}
3	(−57°,−30°)	1687	1674								1721	1727
	(9.5°)	(9.3)	(7.0)								(10.0)	(8.5)
5	(−57°,−31°)	1695	1681	1686	1680						1715	1724
	(9.5°)	(0.0)	(0.0)	(3.0)	(9.0)						(5.5)	(6.5)
8	(−57°,−31°)	1688	1688	1688	1688	1688	1677	1677			1713	1723
	(9.3°)	(0.0)	(0.0)	(0.0)	(0.0)	(0.0)	(2.5)	(2.5)			(6.0)	(7.5)
10	(−57°,−33°)	1687	1687	1687	1687	1687	1687	1687	1676	1676	1713	1723
	(8.5°)	(0.0)	(0.0)	(0.0)	(0.0)	(0.0)	(0.0)	(0.0)	(2.5)	(2.5)	(6.0)	(7.5)

[a] Average dihedral angles (ϕ, ψ) and their standard deviations (σ_φ, σ_ψ), amide-I local mode frequencies excluding hydrogen bonding effects $\bar{\omega}_0$ standard deviations of $\bar{\omega}_0$ due to inhomogeneity of solvation (σ), and the central frequency and inhomogeneity of urethane C═O (ω_U, σ_U) and ester C═O (ω_E, σ_E).

configuration was calculated using the following equation and orientation factor:

$$S^{RPE}_{b-c-a}(\omega_T, \omega_t; \tau) = \left\langle \sum_{i,j,k} \frac{e^{-i\omega_i\tau-\gamma\tau} O_{i,j,k}}{i(\omega_T - \omega_{k0}) - \gamma''} \left[\frac{1}{i(\omega_t - \omega_j) - \gamma} - \frac{1}{i(\omega_t - \omega_{kj}) - \gamma'} \right] \right\rangle \quad (4)$$

$$O_{i,j,k} = \frac{1}{15}[(\boldsymbol{\mu}_i \cdot \boldsymbol{\mu}_j)(\boldsymbol{\mu}_{ik} \cdot \boldsymbol{\mu}_{jk}) + (\boldsymbol{\mu}_i \cdot \boldsymbol{\mu}_{jk})(\boldsymbol{\mu}_j \cdot \boldsymbol{\mu}_{ik}) + (\boldsymbol{\mu}_i \cdot \boldsymbol{\mu}_{ik})(\boldsymbol{\mu}_j \cdot \boldsymbol{\mu}_{jk})] \quad (5)$$

Here subscripts i and j represent the one-quantum states and k the two-quantum states. The transition frequency (moment) between the ground and ith one-quantum states, and between the ith one-quantum and kth two-quantum states is $\omega_i(\boldsymbol{\mu}_i)$ and $\omega_{ki} = \omega_k - \omega_i(\boldsymbol{\mu}_{ik})$, respectively. The homogeneous dephasing of the vibrational coherence is parametrized by Lorentzian line widths γ, γ', and γ'' for the 0–1, 1–2, and 0–2 transitions, respectively. We set $\gamma = 4.5$ cm^{-1}, a typical value for the amide-I band. For transitions involving two-quantum states, we set $\gamma' = 6$ cm^{-1} and $\gamma'' = 10$ cm^{-1} to take into account deviations from the harmonic approximation. The ratio of 2.2 between γ'' and γ is reasonably close to that reported for polyatomic molecules.[69] The angle brackets in eq 4 represent the ensemble average over the inhomogeneous conformational distribution. To perform sufficient sampling of conformations, 25 000 different peptide structures were generated where the dihedral angles of each peptide unit followed Gaussian distributions centered at an average value (φ, ψ). The static disorder of the peptide backbone, as characterized by the standard deviations of the dihedral angles (σ_φ and σ_ψ), gives rise to the disorder in local mode frequencies as well as coupling constants.

When applying the above model to short 3_{10}-helices, we made several assumptions, depending on the peptide chain length. For the tripeptide, the two amide-I local modes cannot form any intramolecular hydrogen bond and hence are exposed to solvent. For such a short peptide, its solution structure is likely to be more floppy and thus deviates from the crystal structure. Therefore, ω_p^0 in eq 1, as well as frequency inhomogeneity and the average dihedral angles, is fully adjusted in the spectral simulations. In the case of longer chain peptides (n = 5, 8, and 10), the 3_{10}-helical conformation is nearly or completely developed.[15] We assumed that all peptide linkages in the chain adopt the same averaged dihedral angles, which are close to the values from a statistical analysis of the crystal structures of peptides containing at least one C^α-tetrasubstituted α-amino acid.[1] For the pentapeptide, we allowed $\bar{\omega}_0$ to be adjusted for each site to extract the best set of local mode frequencies that can reproduce the 2D IR spectra. For the octapeptide and decapeptide, it is impossible to vary $\bar{\omega}_0$ for all sites. Instead, we set $\bar{\omega}_0$ of the last two amide-I modes at the C-terminus to one value and $\bar{\omega}_0$ of the rest of the amide-I modes to another value. These two values were allowed to vary independently. This assumption is reasonable because only the N−H site of the first amide-I mode at the N-terminus and the C═O sites of the two amide-I modes at the C-terminus are exposed to solvent. We have previously shown that the solvent-induced amide-I frequency shift at the N-terminus can be neglected because it has only very minor effects on the simulated spectra.[46]

The capping urethane and ester C═O groups were also incorporated into the exciton model because they partially overlap with the amide-I band, especially for the shorter peptides (n = 3 and 5). Because an *ab initio* map does not exist for the capping groups, we used the amide-I *ab initio* map to approximate the nearest neighbor couplings between the ester C═O group and the C-terminal amide-I mode in the simulation. To calculate the transition dipole couplings, the transition dipole vector of the ester carboxyl group was set parallel to the C═O bond[70] and placed at the middle point of the bond.[71] The same *ab initio* map and transition dipole parameters were used to model the couplings between the urethane C═O group and the amide-I modes. The transition frequencies, static inhomogeneity, and transition dipole derivatives of the capping C═O groups were varied to obtain a good fit to the observed band at >1700 cm^{-1} in the FT IR spectra.

Table 1 lists the optimized parameters resulting from the simulations. The average values of the local mode frequencies (ω_p^0) and the standard deviations are plotted in Figure 2. These parameters were chosen to best reproduce the experimental spectra in eight different formats simultaneously: linear spectra; 2D $\langle Z, Z, Z, Z\rangle$ absorptive spectra; real part R and NR spectra; absolute magnitude R, NR, and RPE spectra; and 2D $\langle \pi/4, -\pi/4, Y, Z\rangle$ absolute magnitude R spectra.

Results

Figure 3 exhibits the FT IR spectra of Z-$(Aib)_n$-O*t*Bu (n = 3, 5, 8, and 10) in $CDCl_3$ (solid lines). Each spectrum is

(70) Tsuboi, M. *J. Polym. Sci.* **1962**, *59*, 139.
(71) Kim, Y. J.; Chang, H.-C.; Sullivan, V. S.; Jonas, J. *J. Chem. Phys.* **1999**, *111*, 9658.

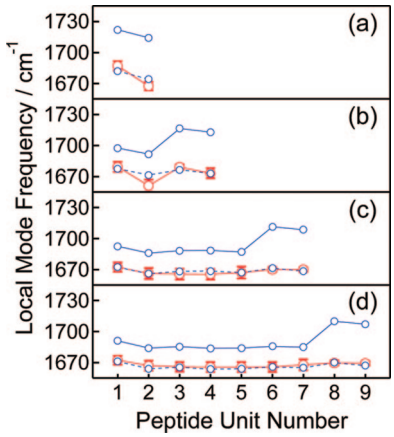

Figure 2. Average amide-I local mode frequencies (ω_p^0, red) used to simulate the linear and 2D IR spectra of Z-(Aib)$_n$-O*t*Bu in $CDCl_3$: $n = 3$ (a); 5 (b); 8 (c); and 10 (d). The peptide units are numbered from the N- to C-terminus. The bar on each symbol indicates the standard deviation of the frequency originating from conformational fluctuation (σ_φ and σ_ψ) and inhomogeneity of solvation. The scaled local mode frequencies (ω_{scaled}, blue circles with solid lines) obtained from AM1 calculated C═O bond lengths are also shown. The peptide backbone is held at the fixed (−57°, −30°) dihedral angles during the geometry optimization process. After lowering the frequencies of the last two units by 20 cm^{-1} to account for enhanced solvent exposure at the C-terminus, the frequencies of the entire curves are red-shifted by 20 cm^{-1} (blue circles with dashed lines).

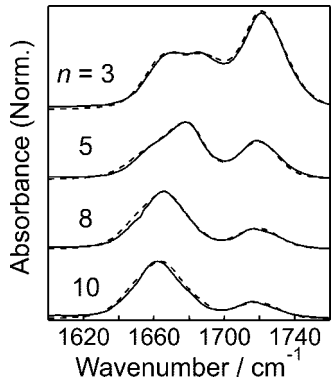

Figure 3. FT IR spectra of Z-(Aib)$_n$-O*t*Bu in $CDCl_3$ (solid lines, $n = 3$, 5, 8, and 10 from top to bottom). Each curve is normalized by the maximum absorbance of the amide-I band at 1660–1685 cm^{-1} after subtracting the neat $CDCl_3$ spectrum. Simulated spectra are shown in dashed lines. The measured and simulated spectra for $n = 3$, 5, and 8 are shifted upward for clarity.

normalized by the maximum absorbance of the amide-I band around 1660–1685 cm^{-1}. The protecting urethane and *tert*-butyl ester C═O groups are not resolved, and one apparent peak shows up at 1718–1720 cm^{-1}. For $n = 3$, the amide-I band exhibits two partially resolved peaks at 1671 and 1685 cm^{-1} that are weaker in intensity than those of the protecting C═O groups. The amide-I spectral shape of $n = 5$ is quite different from that of $n = 3$. A peak appears at 1678 cm^{-1}, and a weak shoulder is observed at ~1656 cm^{-1}. For $n = 8$, a single amide-I band occurs at 1666 cm^{-1} with a full width at half-maximum of 32 cm^{-1}. No other discernible shoulder is observed. For $n = 10$, the amide-I peak position is red-shifted to 1662 cm^{-1} but the line shape and width do not differ from $n = 8$. The peak positions of the amide-I band and terminal C═O groups are in good agreement with those reported previously.[16,29] The simulated linear spectra are overlaid with the measured spectra

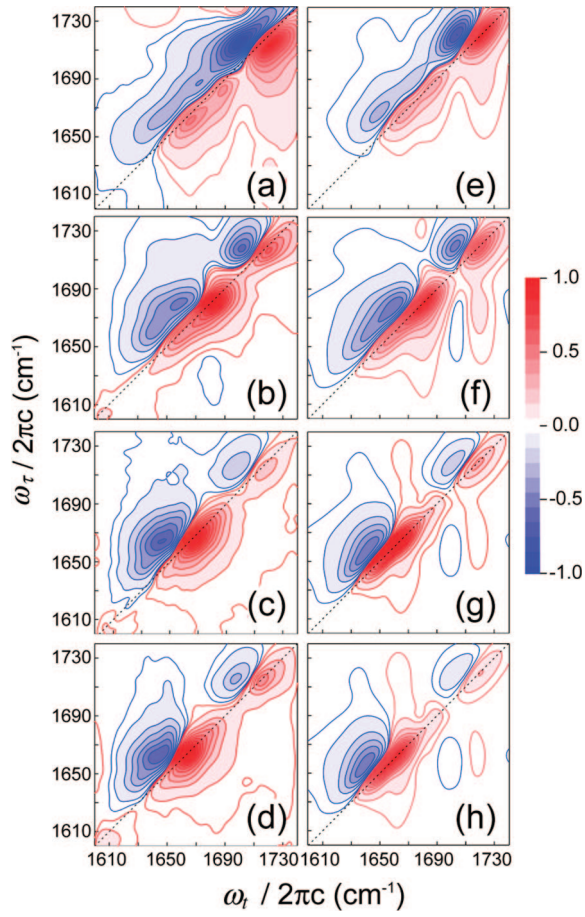

Figure 4. Measured (a−d) and simulated (e−h) 2D absorptive spectra of Z-(Aib)$_n$-O*t*Bu in $CDCl_3$ with the $\langle Z, Z, Z, Z\rangle$ polarization configuration at $T = 300$ fs: $n = 3$ (a, e); 5 (b, f); 8 (c, g); and 10 (d, h). Each spectrum is normalized by the maximum intensity of the positive peak. Contour lines are drawn at 1.5% and from 5 to 95% with 10% increment.

in Figure 2. They reproduce well the observed features for all chain lengths.

Figure 4 shows the measured and simulated 2D absorptive spectra. The positive peaks on the diagonal line involve coherences between the ground and the one-quantum states. The negative peaks are red-shifted from the diagonal along the ω_t axis because they involve evolutions of coherences between the one-quantum states and the anharmonically shifted two-quantum states during the t period. The nodal lines between the positive and negative peaks are all tilted toward the diagonal line. This tilting away from the vertical axis signifies the presence of spectral inhomogeneity that can result from peptide conformational distributions. In the absorptive spectra for $n = 3$ and 5, two closely spaced peaks were observed in the amide-I frequency region. As the peptide chain lengthens to $n = 8$ and 10, a single pair of positive and negative amide-I peaks appeared in the absorptive spectra and they look the same between $n = 8$ and 10.

The real parts of the R and NR spectra that were summed up to give the absorptive spectra are separately plotted in Figures 1S and 2S in the Supporting Information. The R and NR spectra are quite different because the reverse ordering of the first two pulses has very different effects on coherence evolution. First, the nodal lines between the positive and negative peaks in the R and NR spectra are oriented parallel and perpendicular to the diagonal line, respectively. Second, for diagonal peaks that

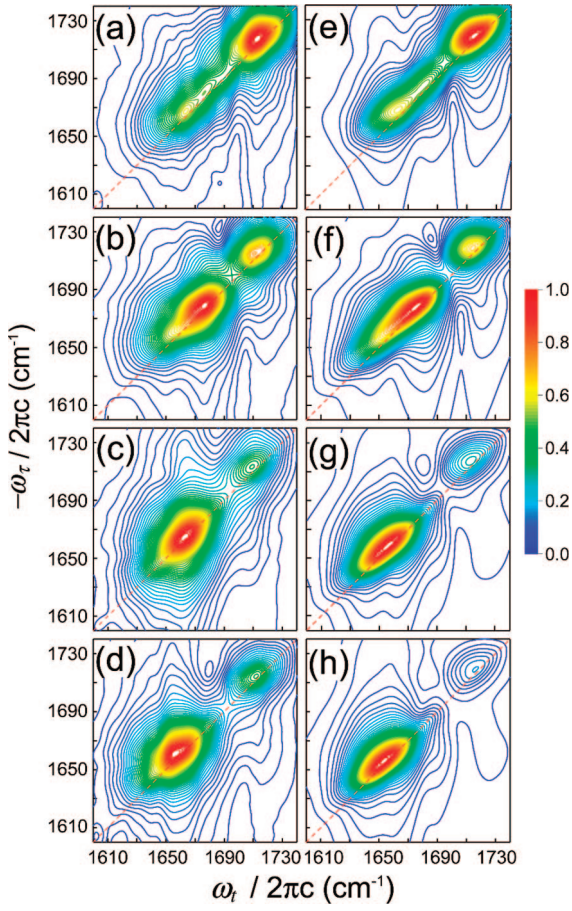

Figure 5. Measured (a−d) and simulated (e−h) absolute magnitude 2D R spectra of Z-(Aib)$_n$-O*t*Bu in $CDCl_3$ with the ⟨*Z*, *Z*, *Z*, *Z*⟩ polarization configuration at $T = 300$ fs: $n = 3$ (a, e); 5 (b, f); 8 (c, g); and 10 (d, h). Each spectrum is normalized by the maximum intensity and drawn with 40 equally spaced contour lines.

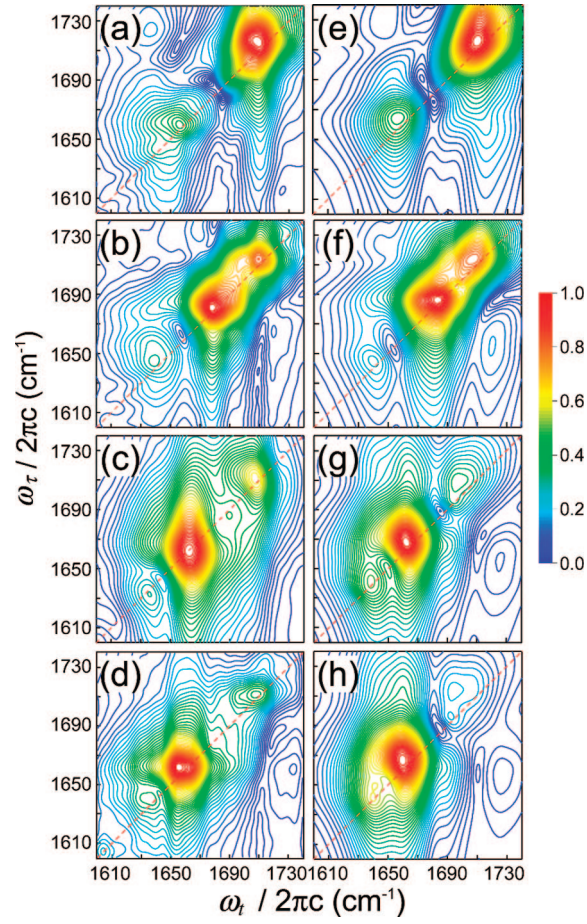

Figure 6. Measured (a−d) and simulated (e−h) absolute magnitude 2D NR spectra of Z-(Aib)$_n$-O*t*Bu in $CDCl_3$ with the ⟨*Z*, *Z*, *Z*, *Z*⟩ polarization configuration at $T = 300$ fs: $n = 3$ (a, e); 5 (b, f); 8 (c, g); and 10 (d, h).

involve the same transitions during the τ and t periods, the dephasing of vibrational coherence due to spectral inhomogeneity can be rephased in the R sequence but not in the NR sequence. This leads to line narrowing in the antidiagonal direction for the diagonal peaks in the R spectrum but not in the NR spectrum. Thus, the absorptive spectrum of an inhomogeneously broadened system can be dominated by the contributions from the R spectrum because of its higher diagonal peak intensity. In fact, the measured R spectra are about 2.5–3.6 times stronger in their amide-I band intensity compared to the NR spectra. Examining the R and NR contributions separately, and comparing them with the simulation, can provide us with more spectral constraints than the absorptive spectrum alone. It is evident from Figure 2S that the NR spectrum exhibits many fine spectral features that are not discernible in the absorptive spectrum. Some of these features manifest as clearly resolved peaks in the absolute magnitude spectra (see below). The agreement between the measured and simulated R and NR spectra is acceptable for all chain lengths.

The 2D IR absolute magnitude spectra, collected with the R, NR, and RPE pulse sequences, are presented in Figures 5−7. In the amide-I region, the R spectrum for $n = 3$ exhibits two partially resolved peaks, the $n = 5$ exhibits a strong peak with a shoulder at the lower frequency side, and the $n = 8$ and 10 exhibit one strong peak (Figure 5). The peak positions in the R spectra along the ω_τ axis are basically the same as those in the FT IR spectra. The amide-I region of the NR spectra is quite different from that of the R spectra. The $n = 3$ exhibits one peak with shoulders on both sides of the diagonal. The main peak is lower in frequency than the two peaks in the R spectrum (Figure 6). The NR spectra for $n = 5$, 8, and 10 show two clearly resolved amide-I peaks along the diagonal, and the frequency separation between two peaks decreases as the chain length increases. The distinct differences between the R and NR spectra stem from the very different orientations of the nodal lines in the complex spectra (Figures 1S and 2S). When multiple vibrators are present in the system and their frequency separations are comparable to the line widths, constructive interference between overlapping peaks of the same sign can lead to broad spectral features elongated along the diagonal line in the absolute magnitude R spectrum. However, destructive interference between overlapping peaks of opposite signs can give rise to well-resolved spectral features in the absolute magnitude NR spectrum.[72] This property has been applied to resolve multiple conformations of a terminally blocked amino acid with two amide-I modes.[41] The R and NR spectra in Figures 5 and 6 are another manifestation of this effect in a more complex system with multiple amide-I vibrators. Comparing the experimental NR spectra in Figures 6 and 2S, it appears that presenting the NR spectra in the absolute magnitude format can provide certain

(72) Ge, N.-H.; Zanni, M. T.; Hochstrasser, R. M. *J. Phys. Chem. A* **2002**, *106*, 962.

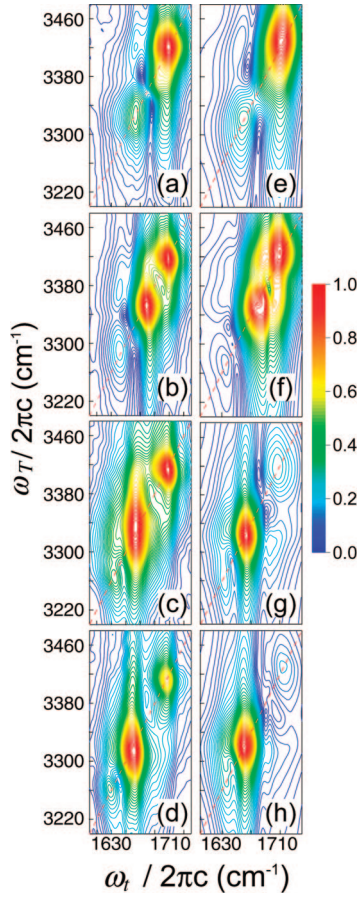

Figure 7. Measured (a−d) and simulated (e−h) absolute magnitude 2D RPE spectra of Z-(Aib)$_n$-O*t*Bu in $CDCl_3$ with the ⟨*Z*, *Z*, *Z*, *Z*⟩ polarization configuration at τ = 300 fs: n = 3 (a, e); 5 (b, f); 8 (c, g); and 10 (d, h).

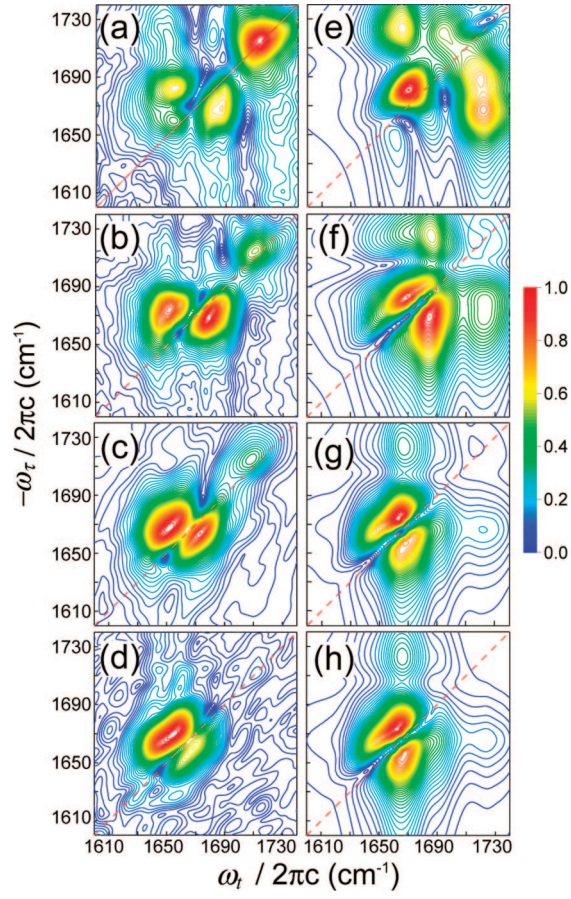

Figure 8. Measured (a−d) and simulated (e−h) cross-peak patterns of Z-(Aib)$_n$-O*t*Bu in $CDCl_3$ with the double-crossed ⟨π/4, −π/4, *Y*, *Z*⟩ polarization configuration at T = 0: n = 3 (a, e); 5 (b, f); 8 (c, g); and 10 (d, h).

advantages. The destructive interference between transitions and its chain length dependence are observed more clearly.

For the RPE spectra, the n = 3 exhibits only one amide-I peak, whereas n = 8 and 10 exhibit a strong peak and a weak peak (Figure 7). The spectrum for n = 5 starts to resemble the patterns of the longer chains. The evolution of the spectral pattern as a function of chain length is similar to that observed in the absolute magnitude NR spectra (Figure 6) because the RPE pulse sequence is also nonrephasing in nature.[41] Destructive interference between closely spaced diagonal peaks can also result in valleys in the absolute magnitude RPE spectra. The main difference between the two types of pulse sequences is that spectral features in NR spectra are elongated similarly along the ω_τ and ω_t axes, whereas the RPE spectra are more elongated along the ω_T axis than along the ω_t axis. This difference in line shape comes from the fact that the 0–2 coherences typically decay faster than the 0–1 and 1–2 coherences. Because the RPE sequence probes the 0–2 coherences during T, it can provide direct measurements of two-quantum dynamics as well as anharmonicities. A recent theoretical study suggests that the RPE spectrum is more sensitive to vibrational couplings than the R spectrum.[56]

The 2D IR spectra measured under the parallel polarization configuration delineate how the spectral pattern of the 3_{10}-helix peptide evolves with chain length. However, it is almost impossible to definitely elicit the frequency position, intensity and shape of the cross-peaks from the spectrum measured with ⟨*Z*, *Z*, *Z*, *Z*⟩, when strong diagonal peaks are not sufficiently separated from cross-peaks. To clarify the chain length dependence of the cross-peak pattern, we measured the absolute magnitude of the R spectrum for n = 3, 5, and 10 under the double-crossed polarization and compared them with the doublet pattern that we had previously observed for n = 8, which we attributed to be the characteristic signature of the 3_{10}-helix.[46] The cross-peak pattern for n = 3 exhibits three peaks (Figure 8a). The weakest peak, close to the diagonal, merges with the two stronger peaks and evolves into a doublet peak pattern as the chain length increases. The simulated pattern exhibits a slightly distorted doublet peak in the amide-I frequency region for n = 5, 8, and 10. Cross-peaks between the amide-I mode and the capping C═O modes are weak in the measured spectra, but they are clearly seen in the simulated spectra.

Discussion

The measured 2D IR spectra of Z-(Aib)$_n$-O*t*Bu/$CDCl_3$ (n = 3, 5, 8, and 10) provide insight into the chain length dependence of the spectral pattern for the 3_{10}-helical conformation. The observed spectra were simulated reasonably well based on the amide-I vibrational exciton model. Below we will discuss the results in detail.

The 2D spectral patterns of the tripeptide are significantly different from the others. The differences are partially due to the small number of the local modes. The tripeptide has two amide-I local modes, and the only relevant coupling constant is the nearest neighbor coupling ($\beta_{1,2}$). Based on Cho's map,[64]

the nearest neighbor coupling strength is 1.1 cm^{-1} for the 3_{10}-helix at (φ, ψ) = (−57°, −30°), which is relatively small compared to 5.1 cm^{-1} for the α-helix at (−63°, −42°) and to 5.9 cm^{-1} for the antiparallel β-sheet at (−139°, 135°). The quite weak coupling in the tripeptide also made it relatively difficult to cleanly observe the cross-peaks under the $\langle \pi/4, -\pi/4, Y, Z\rangle$ polarization configuration as compared to the longer peptides.

The pentapeptide has four amide-I local modes. They are coupled by not only the nearest neighbor couplings but also longer range interactions from up to three residues away. On the basis of transition dipole interactions, the non-nearest neighbor couplings are estimated to be −2.5 cm^{-1} for $\beta_{p,p\pm2}$ and −2.8 cm^{-1} for $\beta_{p,p\pm3}$, more than twice as large as $\beta_{p,p\pm1}$. That is the main difference from the tripeptide. The spectral patterns of $n = 5$ are different from those of $n = 3$, and they have resemblances to those of $n = 8$ and 10. This implies that a characteristic pattern to the secondary structure appears when its size is large enough to form a unit cell of helix periodicity, which corresponds to an acylated pentapeptide ester sequence (or the equivalent acylated tetrapeptide amide) with three successive β-turn hydrogen bonds for the ideal 3_{10}-helix. Once the helical symmetry is established and prolonged, the pattern becomes insensitive to chain length as can be seen from the very similar peak position and shape of $n = 8$ and 10. This experimental observation corroborates our prediction based on model calculations for the ideal 3_{10}-helix structure.[46] The long-range interactions for $\beta_{p,p\pm4}$ and beyond are weaker than 0.8 cm^{-1} in magnitude. Thus, their presence in the longer peptides does not strongly affect spectral patterns. However, as we discussed in the previous paper,[46] even an 11-residue 3_{10}-helix is still not long enough to form the E_1-mode as previously defined in an infinitely long helix.[73] The evolution of the 2D IR spectra from $n = 5$ to 8 and 10 observed here is for 3_{10}-helices of a medium length. At present it is difficult to experimentally investigate whether a much longer 3_{10}-helix, such as a 20-unit peptide,[57] would exhibit different 2D spectral patterns. Z-$(Aib)_{11}$-O*t*Bu is the longest homopeptide with an available crystal structure to date,[27] whereas poly(Aib) is insoluble in most solvents.[74] Because the 3_{10}-helix structure in proteins is usually one to three turns long,[3,4] the results of our study are pertinent to 3_{10}-helices of realistic chain lengths.

In simulated 2D spectra, relatively strong cross-peaks between the amide-I and capping C═O groups appear, but they are much weaker in our measurements. Also, cross peaks between the amide-I modes and the terminal COOH group were not detected for trialanine in D_2O.[40] It is evident that the amide-I-like coupling model is inaccurate for these terminal groups and a more realistic model is required.

The simulated amide-I local mode frequencies exhibit very interesting site dependencies. For $n = 3$ and 5, we adjusted $\bar{\omega}_0$ of every site for the best fit. The resulting ω_p^0 values are strongly varied by ∼20 cm^{-1} within the chain (Figure 2). For $n = 8$ and 10, $\bar{\omega}_0$ of the last two peptide units at the C-terminus were adjusted independently of $\bar{\omega}_0$ of the other residues. The resulting ω_p^0 shows a mild site dependence that largely reflects the effects of intramolecular hydrogen bonds, especially for the inner region. Cho and co-workers[75] calculated the amide-I local mode frequencies of N-acetylated and C-methylated polyglycine peptides of several different secondary conformations and chain lengths using the Hessian matrix reconstruction method. In their results for the 3_{10}-helix structure ($\varphi = -49°$, $\psi = -26°$) with 3–5 peptide units, the last local mode at the C-terminus is always 20–30 cm^{-1} lower in frequency than the preceding mode. This trend is similar to our results for $n = 3$ and 5. In another study they applied an electrostatic potential model to theoretically predict the amide-I local mode frequencies of α-helical polyalanines with different chain lengths.[76] Their calculations show that the local mode frequency in the inner region of a lengthy chain (>10 residues) is rather insensitive to its position, whereas the local mode frequency near the termini exhibits significant site dependence. The site dependence is attributed to the balance between interactions among peptide linkages and effects of intramolecular hydrogen bonds.[76] The local mode frequencies of the last two amide-I modes at the C-terminus obtained in our study (1674–1686 cm^{-1}, see Table 1; here $\omega_p^0 = \bar{\omega}_0$ for $p = n - 2$ and $n - 1$) are close to the frequencies of free amide-I modes in $CDCl_3$.[33,77] Also observed is an interesting trend that the solvent inhomogeneity of the last two local modes decreases with increasing chain length. This suggests that configurations of solvent molecules may be more limited around the exposing C═O groups in the longer chain.

To gain further insight into the site dependency of amide-I local mode frequency, we performed AM1 calculations[78] with the peptide backbone held at the fixed (−57°, −30°) dihedral angles. Recent studies using various quantum chemistry calculation methods have established a linear relationship between the amide-I local mode frequency and C═O bond length.[75,79] Moreover, such a linear relationship has been shown to be valid even when the less accurate semiempirical AM1 calculation method is employed. Following the relationships developed in ref 79, the AM1 calculated C═O bond lengths ($r_{C=O}^{AM1}$) were converted and rescaled to the amide-I local mode frequencies that are comparable to the accuracy at the HF/6-311++G** level using the equation

$$\omega_{scaled} = A + B r_{C=O}^{AM1} \quad (6)$$

where $A = 10932$ cm^{-1} and $B = 7395.8$ cm^{-1}/Å. The resulting amide-I local mode frequencies are shown in Figure 2. The overall trend of the calculated local mode frequency as a function of peptide unit agrees with that of the simulated frequencies except that the last two peptide units are much higher in frequencies compared to the preceding units. This apparent difference is expected because the last two peptide units of $n = 5$, 8, and 10 as well as both peptide units of $n = 3$ are exposed to solvent. The frequencies obtained from the AM1 calculations *in vacuo* should be red-shifted to take into account the weak hydrogen bonding between the exposed amide C═O sites and solvent molecules. Another discrepancy is that the absolute values of the calculated AM1 frequencies are higher than the simulated frequencies. Because of dielectric effects in solvent, we expect the unperturbed local mode frequency (ω_0) to be lower than the amide-I frequency of 1707 cm^{-1} observed for NMA in N_2 and Ar matrixes.[80] Considering both effects,

(73) Nevskaya, N. A.; Chirgadze, Y. N. *Biopolymers* **1976**, *15*, 637.
(74) Malcolm, B. R.; Walkinshaw, M. D. *Biopolymers* **1986**, *25*, 607.
(75) Choi, J.-H.; Ham, S.; Cho, M. *J. Phys. Chem. B* **2003**, *107*, 9132.
(76) Ham, S.; Hahn, S.; Lee, C.; Kim, T.-K.; Kwak, K.; Cho, M. *J. Phys. Chem. B* **2004**, *108*, 9333.
(77) Baron, M. H.; de Lozé, C.; Toniolo, C.; Fasman, G. D. *Biopolymers* **1978**, *17*, 2225.
(78) Frisch, M. J. et al. *Gaussian 03*; Gaussian, Inc.: Wallingford, CT, 2004.
(79) Lee, C.; Cho, M. *J. Phys. Chem. B* **2004**, *108*, 20397.
(80) Torii, H.; Tatsumi, T.; Kanazawa, T.; Tasumi, M. *J. Phys. Chem. B* **1998**, *102*, 309.

we can make the scaled AM1 curves in Figure 2 overlap quite well with the simulated curves by red-shifting the last two amide-I modes by 20 cm^{-1} and then red-shifting all amide-I modes by another 20 cm^{-1}. The magnitude of frequency shifts required is independent of chain length, consistent with the fact that such solvent effects are universal. The 40 cm^{-1} total red shift as applied to the terminal amide-I modes is consistent with the measured amide-I peak position of 1669 cm^{-1} for NMA in chloroform (a 38 cm^{-1} shift from the matrix value).

The good agreement between the scaled AM1 frequencies and the simulated frequencies, after reasonably accounting for the solvent effects, supports the validity of the simulation parameters. It also suggests that semiempirical calculation methods are promising in providing amide-I local mode frequencies for 2D IR spectral simulations when proper scaling is applied. Several models have been developed to calculate amide-I local mode frequencies based on site dependent electrostatic potentials, fields, and field gradients.[81–85] Using these models and performing static averaging over the structures from molecular dynamics simulations have shown to produce line shapes that are broader than measured.[86] While this problem partly results from neglecting the effect of spectral diffusion, improvements on the accuracy of local mode frequency calculations are also needed. With the rapid advancement in computing power, performing semiempirical or DFT calculations on the peptide embedded in a cluster of solvents for many molecular dynamics simulation snapshots may become feasible. To experimentally validate the simulated amide-I local mode frequencies, one systematic approach is to singly ^{13}C-label every C═O group in the peptides and measure the frequency shift of every isotopomer. A 16-residue β-hairpin has been previously studied in this manner using two isotopomers.[43] We plan to apply this method in the future.

In the above simulations, we succeeded in reproducing the observed spectral signatures by adjusting a single set of dihedral angles that was applied to all peptide residues in the chain. The optimized dihedral angles are very close to the average values obtained from the crystal structure survey of 3_{10}-helical peptides containing C^{α}-tetrasubstituted α-amino acids.[1] Deviations of 5° from the optimized angles give significantly worse agreement no matter how other parameters are readjusted. When other parameters are not adjusted, changing the ψ angle by 3° leads to a large intensity change in the substructure in the absolute magnitude NR and RPE spectra (Figures 6 and 7). To explore whether our data can be simulated by α-helical conformation, we set $(\varphi, \psi) = (-63°, -42°)$[1] for $n = 3$ and 5 and adjusted all other parameters. No reasonable parameters were found in this case. Due to the limited φ, ψ space available to Aib, the solution structure of an Aib homo-oligomer should be quite close to its crystal structure for a 3_{10}-helix. Some fraying of 1–2 residues at the termini is reasonably expected. The shorter chain peptide is expected to exhibit larger structural fluctuations and a higher extent of fraying. These effects are manifested in our model simulations where we see that larger values of $(\sigma_{\varphi}, \sigma_{\psi})$ and larger σ of two C-terminal residues are required to simulate shorter chain spectra. Moreover, the cross peak pattern of $n = 3$ in Figure 8 is not simulated as well as those of the longer chains. We attribute this discrepancy to the higher degree of structural heterogeneity of the tripeptide. Because the tripeptide is fully exposed to solvent and can form one intramolecular hydrogen bond at most, it can be floppier than the longer chain peptides with some population not falling within the single β-turn conformation. Our result supports the idea that the percentage of helical population is likely to decrease with decreasing chain length.[15] The pentapeptide appears to exhibit conformational stability similar to that of the longer peptide. The onset of the 3_{10}-helical structure appears to already occur at the pentapeptide level.

Generally speaking, the simulated 2D spectra are in better agreement with the measured spectra for the parallel polarization configuration than for the double-crossed polarization. For instance, the two maxima in the experimental doublet pattern for $n = 5$, 8, and 10 are aligned more horizontally than the simulation. The cross-peak pattern revealed by the double-crossed polarization is very sensitive to the site energies, couplings, and the underlying peptide conformational distributions. It is clear that theoretical advances beyond the simple model applied here are needed to gain more detailed information such as helical contents from the experimental data.

Concluding Remarks

Two-dimensional IR spectroscopy on the amide-I band of Aib homopeptides has allowed us to probe the onset of the 3_{10}-helical structure and to gain insight into how 2D spectral patterns evolve with the 3_{10}-helix chain length. The pentapeptide exhibits spectral features that are similar to those of the longer 3_{10}-helices but are quite different from those of the tripeptide. The onset of 3_{10}-helix spectral signatures appears to already occur upon the formation of a complete 3_{10}-helical turn, when the number and strength of intermode vibrational couplings and conformational stability in a pentapeptide resemble those in a longer peptide. Using a vibrational exciton model and incorporating hydrogen-bond-induced diagonal frequency shifts, we have satisfactorily simulated the chain length dependent 2D IR spectra. Assuming Gaussian distributions for the backbone dihedral angles, our simulations suggest that the Aib homopeptides adopt the 3_{10}-helical conformation in $CDCl_3$, with average dihedral angles $(\phi, \psi) \approx (-57°, -31°)$ and the width of distributions of ~21°. The average angles and conformational disorder exhibit a slight chain length dependence. The more noticeable difference between the experimental and simulated cross-peak patterns of the tripeptide indicates that it is more flexible than the longer chain peptides with some of the population falling outside the single β-turn conformation.

Our results show that 2D IR spectroscopy is highly sensitive to peptide conformation, disorder, and size. Acquiring 2D IR spectra using multiple pulse sequences and polarization configurations can provide a large set of spectral constraints for structure determination and for testing of theoretical models for diagonal frequency shifts and vibrational couplings. It has been suggested that the local mode frequency distribution of a given protein is critical in determining the amide-I band shape and position.[68] The amide-I local mode frequencies obtained from our simulations show a strong site dependence for short peptides. The general trend is in good agreement with the results from scaled AM1 calculations. We believe that a combination of molecular dynamics simulations and semiempirical calculations with proper scaling will be promising for quantitative simulation and detailed interpretation of amide-I 2D IR spectra.

(81) Ham, S.; Cha, S.; Choi, J.-H.; Cho, M. *J. Chem. Phys.* **2003**, *119*, 1451.
(82) Bour, P.; Keiderling, T. A. *J. Chem. Phys.* **2003**, *119*, 11253.
(83) Schmidt, J. R.; Corcelli, S. A.; Skinner, J. L. *J. Chem. Phys.* **2004**, *121*, 8887.
(84) Hayashi, T.; Zhuang, W.; Mukamel, S. *J. Phys. Chem. A* **2005**, *109*, 9747.
(85) Jansen, L. C. T.; Knoester, J. *J. Chem. Phys.* **2006**, *124*, 044502.
(86) Ganim, Z.; Tokmakoff, A. *Biophys. J.* **2006**, *91*, 2636.

The dependence of 2D spectra on 3_{10}-helix chain lengths as established here represents an important step toward bridging the gaps in developing 2D IR spectroscopy as a robust structural probe. A more complete picture of the relationship between spectral features and helical structure will require further work on temperature and solvent dependence as well as chain length dependent studies on α-helices. These studies will provide a useful baseline for probing the transient intermediate conformations amid the coil-to-helix transition.

Acknowledgment. The authors thank M. Cho, G. Stock, and their co-workers for providing us with their nearest coupling maps in refs 64 and 66. This research was supported by grants from the American Chemical Society Petroleum Research Fund (39148-G6) and the National Science Foundation (CHE-0450045) to N.-H.G.

Supporting Information Available: The real parts of the experimental 2D R and NR spectra with the parallel polarization configuration, as well as the corresponding simulated spectra. This material is available free of charge via the Internet at http://pubs.acs.org.

JA8007165